



## Design principles and biological applications of red-emissive two-photon carbon dots

Pooria Lesani<sup>1,2,3</sup>, Aina Hazeera Mohamad Hadi<sup>1</sup>, Zufu Lu<sup>1,2</sup>, Stefano Palomba<sup>3,4</sup>, Elizabeth J. New<sup>3,5</sup> & Hala Zreiqat<sup>1,2,3</sup>

Carbon dots have been gaining attention in the field of nanobiotechnology due to their superior photostability, high water solubility, ease of synthesis and surface functionalization, chemical inertness, low toxicity, and excellent biocompatibility. They also exhibit good two-photon absorption and unique tunable optical properties across a wide range of wavelengths, from ultraviolet to near infrared endowing them with potential for a variety of biological applications. Recently, there has been a growing interest in the synthesis and development of red-emissive two-photon carbon dots. Here we present recent progress in the design requirements for red-emissive two-photon carbon dots, and review current state-of-the-art systems, covering their applications in bioimaging, biosensing, and photothermal and photodynamic therapy.

Fluorescent molecules have been extensively used in both *in vitro* and *in vivo* biological applications. Fluorescence techniques are non-invasive and have very high sensitivity, excellent spatial and temporal resolution, and exogenously applied fluorophores with longer emission wavelengths can generally be readily distinguished from the largely blue naturally occurring autofluorescence<sup>1</sup>. While fluorescent molecules are most commonly utilized in fluorescence microscopic studies, they are also employed in flow cytometric studies and high-throughput imaging assays. Fluorophores may be incorporated into dyes, or markers delineating cells or sub-cellular organelles, or into fluorescent sensors, which report on chemical aspects of their environment. The fluorescence properties of these systems can also be harnessed for therapeutic applications, such as photodynamic therapy (PDT). Given the widely recognized importance of fluorescent molecules in biomedical research, it is important that the most promising fluorophore classes are identified and optimized.

Over the past two decades, a large array of novel fluorophores has been reported for different biological applications<sup>2–4</sup>. While the field is predominated by small molecule systems, such as rhodamine, fluorescein, and cyanine derivatives, modified fluorescent proteins are a popular choice for intracellular studies<sup>4,5</sup>. There is also a rapidly developing body of work on fluorescent nanomaterials, such as carbon nanotubes, graphene sheets, and semiconductor quantum dots<sup>6,7</sup>. While each of these materials has its own advantages, they collectively suffer from a range of limitations, including poor water solubility, complex synthesis, low photostability, and poor sensitivity and selectivity<sup>7–11</sup>.

Among fluorescent nanomaterials, carbon dots (CDs) have recently been recognized to exhibit outstanding physicochemical properties and biological characteristics that make them highly suitable for application in biology and medicine<sup>12</sup>. Given the nascence of this field, it is of great importance to review the current state of the art and identify the most promising paths for future study.

<sup>1</sup>Tissue Engineering & Biomaterials Research Unit, School of Biomedical Engineering, The University of Sydney, Sydney, NSW 2006, Australia. <sup>2</sup>ARC Training Centre for Innovative BioEngineering, The University of Sydney, Sydney, NSW 2006, Australia. <sup>3</sup>The University of Sydney Nano Institute (Sydney Nano), The University of Sydney, Sydney, NSW 2006, Australia. <sup>4</sup>Institute of Photonics and Optical Science (IPOS), The University of Sydney, Sydney, NSW 2006, Australia. <sup>5</sup>School of Chemistry, The University of Sydney, Sydney, NSW 2006, Australia. ✉email: [pooria.lesani@sydney.edu.au](mailto:pooria.lesani@sydney.edu.au); [hala.zreiqat@sydney.edu.au](mailto:hala.zreiqat@sydney.edu.au)

CDs are quasi-spherical-shaped carbonic nanoparticles (typically <10 nm in size), with a nanocrystalline core of graphitic  $sp^2$  carbon atoms and  $sp^3$  carbon defects<sup>12</sup>. The surface of CDs can be extensively decorated with many functional groups, including peripheral carboxylic/carbonyl, hydroxyl, and amide moieties. CDs exhibit a number of other advantageous properties: superior photophysical behavior, including high quantum yield (QY), tunable optical properties<sup>11</sup>, two-photon absorption (TPA) ability, and high photothermal conversion efficiency upon exposure to electromagnetic field<sup>13</sup>. CDs have synthetic versatility, including the ability to be doped by a variety of atoms and molecules<sup>14</sup> and ease of surface functionalization and passivation<sup>15,16</sup>; good chemical<sup>17</sup>, thermal, and photostability<sup>18</sup>; good biocompatibility<sup>19</sup>; and rapid cellular uptake. These merits led to intensive investigation of CDs for a variety of biological applications in biosensing, bioimaging, and photothermal/photodynamic therapies (PTT/PDT)<sup>13</sup>.

The majority of studies to date have focused on developing single-photon excitable CDs with main absorption, excitation, and emission bands in the ultraviolet to green region of the visible spectrum<sup>20,21</sup>. However, high-energy excitation can cause photobleaching<sup>22</sup>, photodamage<sup>23</sup>, and has limited penetration depth<sup>24</sup>, which adversely affect the performance of such CDs as PDT or diagnostic agents. To overcome these limitations, recent years have seen increased interest in the use of CDs in multi-photon applications, making use of their inherent high absorption cross-sections<sup>24,25</sup>. In TPA, a molecule is excited by simultaneous absorption of two lower energy photons<sup>26</sup>, enabling the development of red-emissive CDs, where the nanoparticles are excited by red to near-infrared (NIR) light<sup>27</sup>. Red-emissive two-photon excitable CDs (RTCDs) are generally biocompatible with minimal overlap with biological autofluorescence, low photobleaching, long photostability, low photodamage to healthy tissues, and good tissue penetration<sup>27–30</sup>, rendering them candidates for enhanced efficiency in therapeutic and diagnostic applications.

While some promising, in this article we critically review recent progress in the development of RTCDs for biological applications. We first discuss the mechanisms behind single- and two-photon fluorescence of RTCDs and then review the design and development of RTCDs and their applications in bioimaging, biosensing, and PTT/PDT.

### Photophysical properties of CDs

CDs have proved to be useful for various applications owing to their excellent photophysical, physicochemical, and biological properties<sup>12</sup>. Among these unique properties, the ability of CDs to emit upon two-photon excitation (TPE) holds promise for *in vitro* and *in vivo* biological applications.

**Two-photon fluorescence of CDs.** Traditional fluorescence techniques utilize single-photon behavior, in which a fluorescent molecule in its ground state ( $S_0$ ) absorbs a single photon of light, resulting in the excitation of electrons to a vibrationally excited level of a singlet excited state ( $S_1$ ) (Fig. 1a)<sup>31</sup>. This is followed by rapid, non-radiative loss of energy to the lowest vibrational state, followed by relaxation to the ground state, accompanied by fluorescence emission<sup>32,33</sup>. The energy of the absorbed photon must approximately match the energy difference between the ground and excited states, also known as the band gap energy<sup>34</sup>. In contrast to single-photon absorption, TPA is a non-linear process in which an electron simultaneously absorbs two low-energy photons (Fig. 1b). Each photon has approximately half the energy and twice the wavelength of the band gap and results in the excitation of valence electrons to excited state<sup>35,36</sup>. Due to the necessity for two photons to reach the fluorescent material at

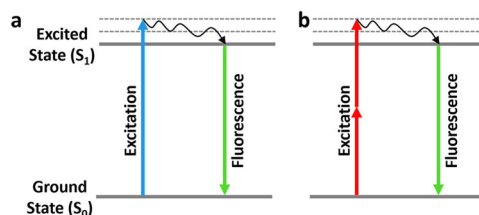


**Fig. 1 Simplified Jablonski diagram for single-photon and two-photon excitation.** **a** Single-photon excitation (blue line) occurs by the absorption of a single photon of light providing sufficient energy to reach the excited state. **b** Two-photon excitation (red line) occurs by simultaneous absorption of two-photon of lower energy. In both cases, subsequent fluorescence emission (green line) emerges when the photons return to the ground state.

approximately the same time, the fluorescence is proportional to the square of the excitation light intensity<sup>36,37</sup>. The non-linearity of the TPA and excitation process can prevent the absorption of photons above and below the focal point and avoid out-of-focus fluorescence<sup>38,39</sup>.

The origin of the CD fluorescence upon single-photon excitation (SPE) and TPE can be attributed to the (i) transition of delocalized electrons in the  $\pi$ -bonding electron cloud of C=C bonds to  $\pi^*$ -antibonding electron bands, and (ii) transition of lone pair electrons from n-nonbonding electron bands to  $\pi^*$ -antibonding electron bands<sup>40,41</sup>. Therefore, it can be expected that CDs show almost similar maximum emission wavelength upon SPE and TPE (Table 1)<sup>42–53</sup>. There are some studies that reported the differences in CD emission maxima after SPE and TPE (Table 1)<sup>54–56</sup>. These differences can be related to the inconsistency in the sum of the energy of the photons used in SPE and TPE, resulting in activation of different emission sites within individual CDs.

The most obvious advantage of two-photon excitable CDs is that the use of longer excitation wavelengths will enable greater depth penetration. This will also minimize photodamage and photobleaching, aided by the limited excitation beyond the focal point<sup>54</sup>. Another advantage is that since no photon absorption takes place above or below the focal plane, the laser beam intensity will be stable<sup>57</sup>. Furthermore, TPE regimes enable the use of short-pulsed lasers with a low incident light that can avoid further damage to the cells and tissues<sup>28</sup>.

**Design considerations for red-emissive two-photon CDs.** The preparation of effective RTCDs for biological applications requires the ability to control the photophysical properties, including high photostability for long-term imaging<sup>58</sup>, high selectivity<sup>59</sup>, and strong photon conversion efficiency and photoactivity<sup>60,61</sup>. In addition, one of the most important photophysical properties of RTCDs is a high TPE efficiency in the red/NIR region<sup>34,62,63</sup>. This is determined by two main factors: (i) the TPA cross-section ( $\delta$ ), which measures TPE efficiency (unit = Goepfert-Mayer (GM), where  $1 \text{ GM} = 10^{-50} \text{ cm}^4 \text{ s photon}^{-1}$ ); and (ii) the fluorescence QY,  $\phi$ , which is the ratio of the number of photons emitted to the number of photons absorbed<sup>62,64</sup>. The product of these two photophysical properties is termed the TPA action cross-section ( $\delta \times \phi$ ), which represents the strength of TPA<sup>65</sup>. A large TPA action cross-section can enable imaging at a low CD concentration without significantly affecting the brightness of fluorescence emission at deep penetration depths<sup>27,62</sup>. Using lower CD concentrations can also reduce potential cytotoxic effects. Two-photon CD-based probes with a large TPA action cross-section can produce strong fluorescence at low short-pulsed laser powers, further minimizing photodamage and photobleaching<sup>64</sup>.

**Table 1 Summary of synthesis methods and properties of RTCDs.**

Synthesis method	Carbon source	Solvents	CD size (nm)	TPA cross-section (GM)	$\phi$ (%)	$\lambda_{ex}$ (nm)	$\lambda_{em}$ (nm)	TP $\lambda_{ex}$ (nm)	TP $\lambda_{em}$ (nm)	Lifetime (ns)	Ref.
Hydrothermal	p-Phenylenediamine, o-phenylenediamine, dopamine	HCl solution	4–5	n.d.	25	573	640	690	640	n.d.	42
	Polythiophene (PT2), diphenyl diselenide	NaOH solution	20	~30,045	17.5	460	731 and 820	880	730 and 800	3.9	43
	Phenylenediamine, dopamine	Water	7.8	1174	26.28	540	665 and 701	800	660 and 701	3.679	44
	p-Phenylenediamine	n.d.	10	103.4	3–10.4	440–580	620	740	~640	2.5–4.42	45
	Lysin, o-phenylenediamine	H <sub>2</sub> SO <sub>4</sub>	9	n.d.	12.4	600	630	808	630	n.d.	46
	Thiourea, o-phenylenediamine	Water	~3.6	~31.5	n.d.	580	615	960	615	n.d.	47
	p-Phenylenediamine	H <sub>2</sub> SO <sub>4</sub>	~5.0	n.d.	21.4	300–580	600	850	602	n.d.	48
	p-Phenylenediamine	DMF	4–11	n.d.	26	561	640	1400	654 and 768	n.d.	54
	Citric acid, urea	NH <sub>4</sub> F	1.5–4	7500	9.8	550	658	960–1060	753 and 846	6.8	55
	Citric acid	Acetone	~2.7	n.d.	31	380–680	673	750	675 and 705	6.8	56
Microwave	Dry taxus leaves	Ethanol	~4.0	~1450	15.1	546	605	700	605	n.d.	49
	p-Aminoazobenzene	Formamide	2.9	n.d.	16.8	420	683	850	683	4.52	50
	Glutathione	Formamide	2.5–5.5	n.d.	22.9	540	640	800–1000	650	0.68	51
Carbonization/pyrolysis	Citric acid, urea	DMF	2–6	n.d.	11.0	732	770	808	784	0.41, 0.56	52
	o-Phenylenediamine, AlCl <sub>3</sub> ·6H <sub>2</sub> O	Solvent-free	1.5–3.5	n.d.	~57.0	532	590, 640, 700	800	560–610, 610–700	3.34–3.42	53
	Tetra-amino porphyrin, citric acid	Water	3.3	n.d.	8.5	440	750	800	n.d.	n.d.	115

TPA two-photon absorption,  $\phi$  quantum yield,  $\lambda_{ex}$  excitation wavelength,  $\lambda_{em}$  emission wavelength, TP two photon, DMF dimethylformamide, n.d. not determined.

A general design principle for two-photon fluorescent probes is the incorporation of electron-donor (D) and electron-acceptor (A) components connected through a  $\pi$ -electron bridge<sup>66</sup>. The intramolecular charge transfer (ICT) process between D and A moieties has been identified to be a primary driving force in TPA<sup>67</sup>, whereby tuning of the strength and conjugation length between the donor and acceptor groups can modify the extent of ICT upon excitation<sup>68</sup>. There have been outstanding reports of how TPA cross-sections can be enhanced by modifying the ICT process through (i) creation of symmetric molecular structure motifs<sup>69</sup>, (ii) incorporation of strong D–A groups<sup>70</sup>, and (iii) expansion and elongation of  $\pi$ -conjugation pathway in a unidirectional way in the molecular structure of the probe<sup>44,69</sup>.

Lan et al.<sup>43</sup> demonstrated that selection of precursors with large  $\pi$ -conjugated systems can lead to enhanced ICT effects, yielding a large TPA cross-section. This can be achieved by co-doping CDs with non-metallic or metallic heteroatoms<sup>71,72</sup>. The doping of CDs leads to the expansion of the conjugated sp<sup>2</sup> domains within the carbon core, increase the charge density, and charge transitions between the graphitic lattice and dopants; increases the number of surface defects and the degree of graphitization; and reduces the non-radiative recombination phenomenon. This not only gives rise to a large two-photon cross-section but also results in high QYs. In a study, it was demonstrated that the manganese-doped CDs showed enhanced fluorescence performance, increased QY, and a red-shift in excitation and emission wavelengths, compared to undoped CDs<sup>73</sup>. Using this method, a number of two-photon CDs have been prepared with  $\delta$  values as high as 50,000 GM<sup>62</sup>. For example, a recently reported nitrogen and fluorine co-doped non-benzene ring-based system showed a significant red-shift in the emission and an almost doubled TPA efficiency, compared to analogous undoped CDs<sup>55</sup>. In another study, the developed RTCDs was based on a graphitic lattice doped with sulfur and selenium and demonstrated a remarkable TPA cross-section of >30,000 GM<sup>43</sup>.

Surface passivation and doping of CD-based fluorescent probes with heteroatoms can also significantly enhance the fluorescence emission intensity and QY<sup>74</sup>. The presence of dopants can reduce the number of carboxyl and epoxy groups present on the surface of CDs leading to non-radiative recombination, a phenomenon that can decrease fluorescence efficiency and  $\phi$ <sup>14,75</sup>. In addition, longer emission wavelengths can be obtained for CDs containing dopants in their graphitized sp<sup>2</sup>-conjugated domains<sup>76</sup>. The dopants can produce defects on the surface of CD-based probes and enhance the degree of graphitization. The higher degree of graphitization induces a red-shift in excitation/emission of CDs, resulting from the enhanced degree of  $\pi$ -conjugation and the decreased bandgap<sup>77,78</sup>.

To date, red-shifted emission and TPA activity of CDs tend to be a fortunate outcome of established synthetic methods, rather than a specific focus of synthetic design. However, examination of RTCDs reported to date can reveal general design principles, which can ensure more targeted synthesis in the future. In particular, careful choice of synthetic parameters can ensure optimization of three key features: TPA cross-section, fluorescence emission wavelengths, and QY.

We have carried out a comprehensive literature review of RTCDs prepared by different synthetic methods (Table 1). It is well known that the structural heterogeneity and surface characteristics of CDs depend strongly on synthetic routes, carbon sources, and solvents<sup>28</sup>. In general, CDs may be prepared by one of two approaches<sup>79</sup>. Top-down synthesis involves the physical or chemical cutting of macroscopic material sources to produce nano-sized CDs<sup>80</sup>. The bottom-up synthesis approach involves building CDs from molecular precursors, whether by hydrothermal, solvothermal, microwave-assisted, or carbonization methods<sup>81</sup>. Bottom-up

approaches tend to be favored for the synthesis of RTCDs synthesis as they lend themselves to green chemistry alternatives (e.g., from biomass and food wastes)<sup>82</sup>, require less harsh conditions, cheaper reagents, and shorter reaction times than top-down approaches<sup>81</sup>. Furthermore, bottom-up synthetic methods offer great control over the synthesis parameters and particle size distribution<sup>83</sup>.

While the synthetic method plays a key role in determining the final photophysical properties of RTCDs (Table 1), other synthetic and post-synthetic parameters can also significantly influence RTCD chemical composition and photophysical and biological behavior. These include the type of solvent, heating time and temperature, microwave power, starting materials and solvents, and method of purification. The microstructure of the starting material has a direct effect on the microstructure of the synthesized CDs and thus their physicochemical properties. This is due to the fact that the starting material only partially breaks down during the synthesis process, resulting in retention of some aspects of the initial microstructure in the synthesized CDs. In a recent study by Abbas et al.<sup>84</sup>, it was demonstrated that the use of a partially carbonized precursor resulted in the development of CDs, while  $sp^2$  dominant carbon precursors were found suitable for the synthesis of graphene quantum dots. The nature of the solvent, and particularly the polarity, significantly affect the synthesis yield, degree of carbonization, and surface functionality of CDs<sup>59</sup>. Synthesis heating time and temperature can notably affect the optical properties of CDs. These parameters can change the particle size distribution range and the length of conjugated- $\pi$ -systems of CDs, resulting in varying the valence electrons and consequently the highest occupied molecular orbital (HOMO)-lowest unoccupied molecular orbital (LUMO) energy gaps<sup>85</sup>. In addition, optimizing the reaction time and temperature can minimize the amount of unreacted ingredients or overreacted products after the synthesis of CDs<sup>59</sup>. The importance of purification procedures, including dialysis, ultrafiltration, and organic washes, on the physicochemical and optical properties of CDs was investigated by Noun et al.<sup>86</sup>. They demonstrated that CDs synthesized under different conditions using the same starting materials may result in different levels of impurities, with a resulting side products produced with differing size, absorbance, fluorescence, and QY values, inducing heterogeneity in the CD optical properties and surface composition<sup>86</sup>. Therefore, purification profiles and purification requirements on a new CD system must be optimized to achieve high purity of CDs. Particle size distribution can also play an important role in tailoring the optical properties of CDs. To demonstrate the particle size effect on the photophysical and biological properties of CDs, Lesani et al.<sup>59</sup> reported that the separation of synthesized CDs into narrower size distribution ranges minimized the impurities and further optimized the photophysical and biological behavior of CDs. They demonstrated that the increase in CD particle size results in red-shifting of excitation and emission maxima of CDs. Increasing particle size distribution range leads to superior intracellular uptake by the cells, compared to CDs with smaller particle size distributions<sup>59</sup>. The smaller CDs may enter the cells less effectively as they could travel into and out of cells more easily due to their small size<sup>87,88</sup>. Their propensity to passively cross the cell membrane may also explain the lower cellular uptake, as active export mechanisms coupled with an equilibration against the concentration gradient would prevent the accumulation of these CDs within the cells.

Therefore, in order to achieve the highest efficiency and performance for a specific application, it is strongly recommended to evaluate both synthetic and post-synthetic parameters in synthesis and development of different types of CDs. The analysis of the data in Table 1 shows two essential components for the development of RTCDs: (i) presence of at least one

heteroatom in the synthesized RTCDs, (ii) use of carbon source with aromatic rings and heterocycles. The presence of electron-rich aromatic rings (most often heterocycles) can influence the degree of graphitization of the RTCD core and produce more surface defects with efficient  $\pi$ -conjugated systems and thus significantly reduce HOMO-LUMO energy gaps resulting in a red-shift in excitation and emission wavelength with narrow full width at a half maximum, large Stokes shift, and enhanced QY and TPA cross-section<sup>7,14,59</sup>. To further improve the photophysical properties of RTCDs, the presence of a second heteroatom in the structure of RTCDs can further expand the conjugated  $sp^2$  domains within the carbon core and reduce the non-radiative recombination phenomenon<sup>43</sup>. Hydrothermal/solvothermal synthetic methods generally produced RTCDs with higher TPA cross-section and QY values due to the higher graphitization degree and uniform particle size distribution of RTCDs synthesized using these methods. As some characteristics of developed RTCDs in these studies have not been determined, more investigation and characterization are needed for detailed comparison between different synthetic methods' efficiency.

### Biological applications of RTCDs

RTCDs have shown promise across a range of biological applications due to their excellent photophysical properties<sup>12</sup>. In addition, CDs possess good biocompatibility, and this property can be further improved by surface passivation with polymers to significantly reduce protein corona formation and enhance biostability<sup>89-92</sup>. In the following sections, we discuss in detail the application of RTCDs in bioimaging, biosensing, and PTT/PDT applications in complex biological systems.

**Biolabeling.** The elucidation of biological structures, whether individual cells, tissues, or organelles, is crucial for biomedical research and applications. One highly effective method to achieve this is the use of fluorescent biolabels, which accumulate in the region of interest and provide a stable fluorescence output that can be correlated with other imaging data<sup>93-95</sup>. RTCDs have shown promise as fluorescent biolabels mainly due to their bright red/NIR fluorescence and excellent photostability and biocompatibility. This is crucial for the non-invasive real-time monitoring of in vitro and in vivo specimens to understand the biological processes occurring at a cellular and molecular level<sup>42</sup>.

**RTCDs as intracellular stains.** CDs are readily able to cross cell membranes via fluid phase endocytosis, receptor-mediated endocytosis, clathrin-mediated endocytosis, caveolae-mediated endocytosis, phagocytosis, and/or passive penetration<sup>96</sup>. CDs have been reported to localize in a number of different intracellular compartments, including the cytoplasm and cell membrane<sup>24,97</sup>, around and inside the cell nucleus<sup>55,98</sup>, and the nucleolus<sup>99</sup>. Existing literature has concluded that the cellular uptake and intracellular localization of CDs can be influenced by their size, surface functional groups, biocompatibility, and surface charge<sup>100-102</sup>. However, more studies are essential to understand the effect of physicochemical specifications of CDs on their cellular interaction and localization behavior. While there is fewer reports about the biological behavior of RTCDs, much of the information from the CD literature is likely to be applicable.

Zhai et al.<sup>103</sup> used citric acid and 1,2-ethylenediamine in microwave-assisted pyrolysis to synthesize excitation-dependent CDs with the ability to emit at blue, green, and red wavelengths when the excitation wavelength is  $>400$  nm. The excitation dependency of these CDs was attributed to the presence of different functional groups on their surface, each contributing to distinct excitation and emission profiles. These CDs were used for



multicolor cellular fluorescence imaging using different excitation wavelengths of 405, 488, and 543 nm. They were found to rapidly internalize into L929 cells, staining their cytosol<sup>103</sup>. The excitation dependency of CDs could be a disadvantage for bioimaging studies<sup>104</sup>. The emission peak shifts of excitation-dependent CDs with varied excitation wavelengths makes it challenging to choose a suitable bandpass filter during imaging, therefore limiting the sensitivity and linear range of resulting measurements<sup>104</sup>. Excitation-dependent CDs have limited multiplexing capability, as their broad-ranging excitation and emission will overlap with those of other molecules over a broad range of wavelengths<sup>104,105</sup>. While this study<sup>103</sup> did not investigate TPA behavior, the similarity of these CDs to other reported RTCDs suggests that they are also likely to be useful for two-photon microscopy.

Recently, there has been a significant focus on developing CDs with the ability to penetrate into the nucleus and nucleolus of the cells, in line with a general need to better understand nuclear morphology and function<sup>68</sup>. The first CDs with the ability to penetrate into the nucleus of NIH-3T3 mouse fibroblasts cells were reported in 2014<sup>106</sup>. These CDs (~5 nm) were synthesized using thermal oxidation of tris(hydroxymethyl)aminomethane and betaine hydrochloride. These authors hypothesized that the nuclear uptake of CDs is due to passive transport through the nuclear pore complexes (20–50 nm in size). The strong interaction of CDs with nuclear DNA is facilitated by the strong surface positive charge (~+55 mV) of the CDs<sup>106</sup>. This study demonstrated the ability of CDs to not only label the cytoplasm but also the other organelles of the cells inspiring further research to develop red-emissive CDs (RCDs)/RTCDs that target nucleus and/or nucleolus.

More recently, Jiang and co-workers synthesized co-doped RCDs using citric acid (carbon source), urea (nitrogen source), ammonium fluoride (fluorine source), and dimethylformamide (solvent) via solvothermal method<sup>55</sup>. These RCDs possessed strong absorption across ultraviolet–NIR wavelengths (430–760 nm) and excitation-independent bright deep-red emission (777 nm). Real-time confocal laser scanning microscopic imaging of HepG2 cells treated with the RCDs demonstrated rapid cellular uptake. The cytoplasmic and nucleolar fluorescence of RCDs was evident after a short incubation time, with time-dependent accumulation in both regions. This study shows the rapid cellular uptake of the RCDs with simultaneous labeling of the cytoplasm and the nucleolus in live cells. The authors attributed this to the interaction between ribosomal RNA (distributed in both cytoplasm as well as nucleolus) and RCDs with both positive and negative charges on their surface (i.e.,

charge heterogeneity)<sup>55,98,102</sup>. However, the study was only performed in HepG2 cells, which have high ribosomal content due to a rapid rate of cell division, therefore a broader study of other cell types is recommended to confirm the generality of this localization behavior. Additional studies are required to shed light on the mechanisms of RCD–ribosomal RNA interactions. Further, the two-photon imaging capability was not assessed, and further evaluation would be required to confirm that the RCDs enable collection of cell images with two-photon microscopy, providing enhanced distinction between sub-cellular organelles at higher resolution.

Sun et al.<sup>51</sup> were among the first to develop RTCDs using citric acid (carbon source) and formamide (solvent) via a microwave synthesis method. The fabricated RTCDs possess excellent TPE fluorescence using a femtosecond pulse laser with an identical intense emission at  $\lambda_{em} = 650$  nm upon both single-photon ( $\lambda_{ex} = 540$  nm) and two-photon ( $\lambda_{ex} = 850$  nm) excitation. This indicates that the emission in both cases arises from the same excited state. The biolabeling capability of RTCDs was studied by two-photon microscopy in both MCF-7 and HeLa cells. After 4 h incubation, strong emission was observed from the nucleolus of the cells upon TPE at 850 nm (Fig. 2a). The nucleolar staining was attributed to higher affinity of RTCDs to RNA-rich nucleolus than DNA and other substances in cytoplasm. MCF-7 cells pretreated with RNase, which hydrolyzes cellular RNA but not DNA, showed general nuclear staining rather than the puncta typical of nucleoli (Fig. 2b). In contrast, RNase treatment had no effect on Hoechst staining patterns, as this dye stains DNA rather than RNA. These results further confirm that RTCDs have higher affinity for the RNA-rich nucleolus, with good selectivity for identifying the nucleolus from the nucleus. Similar results were also reported for HeLa cells demonstrating the nucleolus-specific labeling capability of RTCDs and the advantage of red-emissive two-photon excitable labeling agent in eliminating autofluorescence from the biological matrix using two-photon fluorescence microscopy.

While not developed for these specific purposes, the RTCDs described above can potentially be used as organelle stains. RTCDs with narrow emission bands could be utilized for colocalization studies with other fluorescent dyes or probes. To date, organelle-specific RTCDs have not been prepared by rational design but instead have arisen from exploratory studies in which newly synthesized RTCDs have been investigated through microscopy, and in some cases a biological or medicinal use retrofitted from the observed activity. In order for the field to move forward, it is essential that structure–function activities are elucidated, enabling the rational design of RTCDs with specific

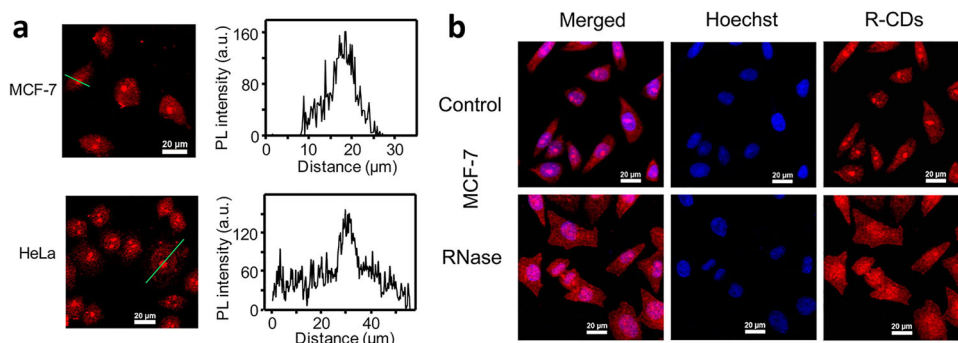


**Fig. 2** The nucleolus-specific labeling capability of RTCDs. Two-photon confocal fluorescent images of cells incubated with RTCDs **a** living MCF-7 cells and HeLa cells, along with corresponding quantitative figure along the green line ( $\lambda_{ex} = 850$  nm fs-pulse laser,  $\lambda_{em} = 600$ –750 nm; scale bar = 20  $\mu$ m). **b** Confocal fluorescent images of the RTCDs and Hoechst without (i.e., control) and with the RNase treatment of MCF-7 cells (Hoechst,  $\lambda_{ex} = 405$  nm,  $\lambda_{em} = 420$ –500 nm; RTCDs,  $\lambda_{ex} = 543$  nm,  $\lambda_{em} = 550$ –750 nm; scale bar = 20  $\mu$ m). (Fig. 2a, b adapted with permission from ref. <sup>51</sup>, Copyright 2016 American Chemical Society).

intracellular behavior. This will require that the mechanisms of cellular uptake and localization of CDs are better understood.

To date, intracellular RTCDs have been reported with localization to the cytoplasm, nucleus/nucleolus, or cell membrane. Therefore, further work is required in targeting RTCDs to the number of other sub-cellular locations including the mitochondria, lysosomes, endoplasmic reticulum, and Golgi apparatus, all critical to the progress of medical research. Given the ease of post-synthetic functionalization, and the well-established peptide and small-molecule targeting groups for key organelles, it should be straightforward to achieve such localization. For example, the mitochondria, central to the health and disease of the cell, can be targeted by the use of lipophilic cationic tags or short peptide sequences<sup>107</sup>.

**RTCDs as markers for in vivo imaging.** In order to be suitable for use in in vivo imaging, a fluorophore must meet a number of criteria. First, long-wavelength excitation and emission is required for sufficient tissue penetration. This can be achieved by using two-photon excitable dyes. Second, the fluorophore should exhibit high photostability to enable long-term imaging. As for cellular dyes, the fluorophore should exhibit good biocompatibility and rapid cellular uptake but additionally must be rapidly cleared post-injection, to reduce retention in heavy vascularized tissues. For fluorophores to be applied to brain imaging, an additional requirement is the ability to cross the blood–brain barrier. RTCDs have attracted considerable attention in recent years for in vivo fluorescence imaging as they can be designed to meet these requirements.

One of the key criteria for CDs for in vivo use is their clearance post-injection, with rapid and efficient excretion, and minimal residual accumulation in heavy vascularized tissues<sup>108</sup>. This is important not just for safety reasons but also to prevent the protein corona formation on the surface of the CDs<sup>18,109</sup>. Yang et al.<sup>89</sup> showed that CDs are primarily cleared by the body through the kidneys and, to a lesser extent, through the liver. In this study, they demonstrated that intravenous injection of murine with CDs (20 mg carbon core-equivalent kg<sup>-1</sup> body weight) only exposed 20 and 2 µg of residual in the liver and spleen, respectively. The findings of other studies point to the rapid clearance of CDs even when administered intravenous, intramuscular, and subcutaneous<sup>110</sup>. Studies of radioactively labeled nanoparticles revealed that 1% of the injected dose remained per gram after all three injection routes, with low levels of accumulation in the reticuloendothelial system<sup>110</sup>.

Li and co-workers performed surface modification of CDs by incorporating poly(vinylpyrrolidone) (PVP) to enhance the density of sulfoxide/carbonyl groups on the surface of CDs<sup>54</sup>. The attachment of these groups to the outer layer of the CDs increases the surface oxidation and the occurrence of discrete energy levels, which results in the development of RTCDs. The surface-modified RTCDs possess a NIR absorption band and efficient NIR emission with either SPE (700–900 nm) or TPE (1000–1700 nm). PVP-treated RTCDs were gavage injected into mice and real-time in vivo fluorescence imaging was performed using a complementary metal oxide semiconductor camera at excitation and emission wavelength of 671 and 750 nm, respectively. After injection of these PVP-treated RTCDs, bright NIR fluorescence (Fig. 3a, b) was observed in the stomach of the mice, revealing the in vivo imaging ability and deep-tissue penetration capability of the developed RTCDs.

In another study, Lu et al.<sup>44</sup> synthesized novel NIR-emissive RTCDs from *o*-phenylenediamine and dopamine with high fluorescence QY ( $\phi$ ) of 26.28% and TPA cross-section ( $\delta$ ) of 1174 GM. They concluded that the fluorescent processes of RTCDs for both single-photon and two-photon fluorescence are similar. The

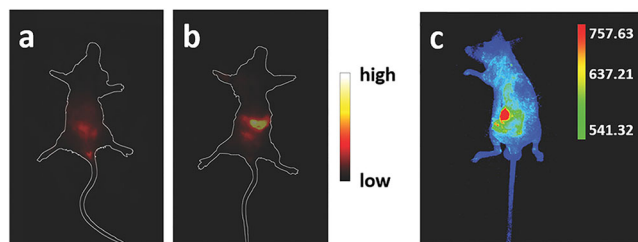


**Fig. 3 In vivo fluorescence imaging capability of RTCDs.** In vivo NIR fluorescence in mouse **a** before and **b** after injection with CDs in PVP aqueous solution ( $\lambda_{\text{ex}} = 671$  nm,  $\lambda_{\text{em}} = 750$  nm). **c** In vivo fluorescence image of nude mice subcutaneously injected with RTCDs ( $\lambda_{\text{ex}} = 540$  nm,  $\lambda_{\text{em}} = 600$  nm). The color bars represent the intensity of fluorescence. (Fig. 3a, b adapted with permission from ref. <sup>54</sup>, Copyright 2017 Wiley. Figure 3c adapted with permission from ref. <sup>44</sup>, Copyright 2018 Wiley).

high  $\phi$  value was attributed to the synergistic effect of the carbon core and the surface state in the fluorescence emission, while the high  $\delta$  value was attributed to the donor–bridge–acceptor dipole structure within large conjugated rigid sp<sup>2</sup> domain. The RTCDs developed in this study were subcutaneously injected into the backs of nude mice yielding excellent fluorescence signal with good signal-to-noise ratio at SPE and emission wavelengths of 540 and 600 nm, respectively (Fig. 3c). However, their study did not determine the tissue penetration ability of the developed RTCDs. In this study, RTCDs, subcutaneously injected, were localized near the nude mice skin, and the fluorescence imaging was performed only using SPE.

These studies demonstrate the potential use of RTCDs as labeling agents for in vivo monitoring of complex biological organs and tissues. However, the effect of their physical properties such as size and shape, and chemical composition, on their interaction with biological systems are yet to be explored. The chemical and photophysical characteristics of RTCDs can significantly influence their biodistribution, bioavailability, targeting efficacy, opsonization, cellular uptake, organ distribution, and clearance kinetics<sup>9,59,102</sup>. Therefore, it is essential to study and optimize these factors in future studies to enhance the efficacy of RTCDs in biological systems. More detailed understanding of these relationships will enable to preparation of bespoke RTCDs for specific in vivo applications in the future.

**Biosensing.** While biolabels are markers of a physical domain, many of the key questions in medical research and the clinic are related to chemical environments and chemical reactions. Biosensors are designed to report on one aspect of the chemical environment, whether through a specific response to an analyte or activation by a chemical reaction. The key criteria for a biosensor are robust response, stability, limit of detection and sensitivity, and target selectivity<sup>24</sup>. Over the past two decades, there have been a large number of biosensors reported based on fluorescence nanomaterials, such as semiconductor quantum dots<sup>6</sup> and metal nanoparticles<sup>111</sup>. RTCDs have received significant attention in the field of biosensing due to their unique optical tunability and red/NIR emission<sup>25</sup>. The excellent photostability, chemical inertness, and good biocompatibility of RTCDs make them promising candidates for real-time tracking, monitoring, and measurement of biological events<sup>104</sup>.

Since many biological analytes of interest are present in very low concentrations in cells, it is important that biosensors have a reasonable limit of detection and can be applied and observed at low concentrations themselves. The surface modification and functionalization of the RTCDs can be readily performed through the passivation, coating, and conjugation of polymers, proteins, biomolecules, and targeting agents with the surface functional

groups of the nanoparticles<sup>24</sup>. This ability can potentially improve the fluorescence sensitivity of the RTCDs to nanomolar levels with excellent selectivity toward the target elements such as metal ions, biomolecules, and pH changes in biological systems.

Ye and co-workers synthesized pH-responsive RTCDs using *p*-phenylenediamine, *o*-phenylenediamine, and dopamine as ingredients and hydrochloric acid as the solvent<sup>42</sup>. These RTCDs show a linear pH response in the range of 3.5–6.5, with fluorescence decreasing with increasing pH. The pH-responsive behavior was attributed to the aggregation–disaggregation of the nanoparticles resulting from deprotonation and protonation of the amino groups on the surface of the RTCDs. The biosensing capability of RTCDs was investigated both *in vitro* and *in vivo*. MCF-7 cells loaded with RTCDs were incubated in buffer solutions of different pH-containing nigericin and monensin to allow equilibration of the cytoplasmic pH with the extracellular medium. Two-photon fluorescence images of the cells (Fig. 4a) show a clear decrease in fluorescence intensity with increasing pH from 4.0 to 7.0 with almost no emission observed at pH 8.0. This trend was also found in zebrafish placed for 2 h in buffer solutions of different pH. Strong red fluorescence emission was observed at acidic pH, with clear fluorescence decreases when the pH was elevated to 8.0 (Fig. 4b). These results exhibit the ability of the developed RTCDs to detect pH both *in vitro* and *in vivo*. However, in this study, the pH operating range is below physiological pH, so it is not likely to be sensitive to biologically relevant perturbations in pH.

In another study, Wang et al.<sup>45</sup> developed RTCDs from *p*-phenylenediamine that were capable of detecting and monitoring the formaldehyde (FA) in living biological systems. The RTCDs showed a linear turn-on fluorescence response toward increasing concentrations of FA, with a detection limit of 9.9  $\mu\text{M}$ . The FA-sensing mechanism of the RTCDs was attributed to the rapid Schiff base formation reaction of the surface amine groups with

FA. The resulting Schiff bases show disrupted hydrogen bond interactions with the solvent, thus overcoming the fluorescence quenching effect of the solvent (Fig. 5a).

These RTCDs were successfully applied for the intracellular FA detection in HepG2 cells incubated with millimolar concentrations of FA and subsequently tested *in vivo* in a zebrafish model. The single- and two-photon fluorescence images of zebrafish incubated with RTCDs ( $50 \mu\text{g mL}^{-1}$ ) demonstrate a weak red fluorescence, compared to untreated controls (Fig. 5b, c, e, f), while zebrafish treated with 5 mM FA showed a clear increase in fluorescence intensity (Fig. 5d, g). It was also reported that RTCDs can be used for FA detection at depths of up to 240  $\mu\text{m}$  upon TPE<sup>45</sup>. While this is sufficient for zebrafish studies, this short depth penetration is likely to limit application in larger organisms.

Overall, these studies demonstrate the capability of RTCDs for use as biosensors for monitoring and quantifying a variety of target elements in *in vitro* and *in vivo* systems. Given the plethora of biologically relevant analytes, there is certainly still much to be achieved in this field. There is a lack of understanding about how to rationally achieve good selectivity and sensitivity of RTCDs, and there is a need to optimize the optical properties of RTCDs, particularly by red-shifting their fluorescence excitation and emission to the second and third NIR windows.

**Phototherapy.** Phototherapy is a therapeutic technique in which specific wavelengths of light are used to treat diseases, such as cancers and infection. PTT and PDT are the two main phototherapy approaches for minimally invasive cancer treatment<sup>112</sup>. In PTT, a photothermal agent is stimulated by light for the selective local heating of the target abnormal cells and tissues. PTT efficiency is dependent on the NIR absorption wavelength and coefficient of the photothermal agent and the power of the excitation light<sup>113</sup>. In PDT, the photoactivated photosensitizer

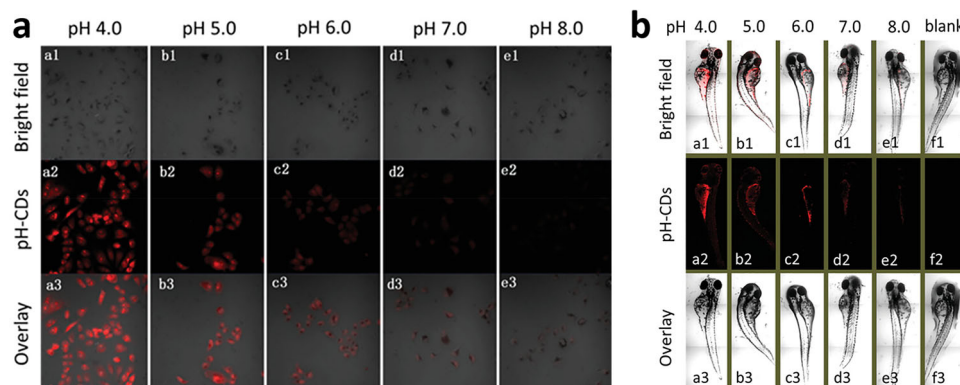


**Fig. 4** *In vitro* and *in vivo* pH sensing using RTCDs. Two-photon fluorescence images of **a** MCF-7 cells and **b** zebrafish incubated with RTCDs (pH-CDs) at different pH values ( $\lambda_{\text{ex}} = 690 \text{ nm}$ ,  $\lambda_{\text{em}} = 620\text{--}660 \text{ nm}$ ). (Fig. 4a, b adapted with permission from ref. <sup>42</sup>, Copyright 2019 Wiley).

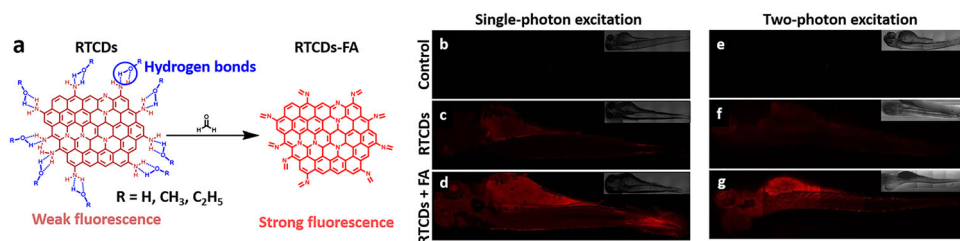


**Fig. 5** RTCD sensing mechanism and *in vivo* sensitivity toward formaldehyde (FA). **a** Possible reaction mechanism of RTCD toward FA. Single-photon (**b–d**) and two-photon (**e–g**) fluorescence images of zebrafishes incubated with RTCDs.  $\lambda_{\text{ex}} = 480 \text{ nm}$  (single-photon,  $\lambda_{\text{em}} = 500\text{--}700 \text{ nm}$ );  $\lambda_{\text{ex}} = 740 \text{ nm}$  (two-photon,  $\lambda_{\text{em}} = 500\text{--}700 \text{ nm}$ ). Scale bar = 400  $\mu\text{m}$ . (Fig. 5a–g adapted with permission from ref. <sup>45</sup>, Copyright 2019 Elsevier).



generates a chain of photochemical reactions to produce reactive oxygen species (ROS) leading to cell death. To guarantee the effectiveness of PDT, the photosensitizer should be targeted to the nucleus or mitochondria, regions of the cell most susceptible to ROS damage<sup>114</sup>, as well as a large absorption coefficient in the NIR is required to ensure sufficient tissue penetration<sup>49</sup>. In this regard, RTCDs possess an excellent NIR absorption coefficient with ability to excite and emit in red/NIR regions under exposure to low power laser irradiation resulting in their high efficiency at deeper tissue depths<sup>33</sup>. The surface functionality and tunability of RTCDs can be further utilized in delivering them to the desired cell type and the target organelle to increase the selectivity to only cancerous cells<sup>60</sup>. In addition, good biocompatibility and high photostability of RTCDs can further ensure their applicability in long-term phototherapy and real-time monitoring of phototherapeutic processes<sup>76</sup>. Therefore, due to the promising characteristics of RTCDs, their potential applicability for use as phototherapy agent in PTT and PDT has recently attracted significant attention.

The nucleolar-localized RTCDs developed by Sun et al.<sup>51</sup> and discussed in the section “RTCDs as intracellular stains,” exhibited good NIR absorption (650–880 nm) and high water dispersion and demonstrated the ability to convert laser energy (671 nm laser,  $2.5 \text{ W cm}^{-2}$ ) efficiently and rapidly into heat ( $\sim 60^\circ\text{C}$ ), corresponding to a high photothermal conversion efficiency (43.9%) (Fig. 6a), properties that suggest their suitability as potential PDT agents. In this study, MCF-7 cells were incubated with different concentrations of RTCDs ( $0\text{--}200 \mu\text{g mL}^{-1}$ ) and exposed to laser irradiation for 10 min (Fig. 6b)<sup>51</sup>. Cell viability decreased with increasing RTCD concentration. At high concentrations of RTCDs ( $200 \mu\text{g mL}^{-1}$ ), 100% MCF-7 cell death was obtained after only 6 min laser irradiation. These results suggest the potential use of RTCDs in cancer treatment applications as PTT agents.

In another study, red-emissive two-photon excitable S, Se-co-doped RTCDs were prepared through a hydrothermal method, with polythiophene and diphenyl diselenide as ingredients<sup>43</sup>. The RTCDs show strong ability for converting light energy into heat. The temperature of an aqueous solution containing 160 ppm RTCDs increased up to  $30^\circ\text{C}$  after 10 min laser irradiation ( $635 \text{ nm}$ ,  $2 \text{ W cm}^{-2}$ ), corresponding to a high photothermal conversion efficiency of  $\sim 58.2\%$ . Fewer than 10% of HeLa cells remained viable when incubated with  $80 \mu\text{g mL}^{-1}$  and exposed to laser irradiation for 10 min. Next, two-photon fluorescence imaging was performed to monitor the capability of RTCDs for PTT. HeLa cells incubated with RTCDs demonstrated strong red fluorescence under two-photon laser excitation of  $880 \text{ nm}$  (Fig. 7a). The TPE PTT efficiency was assessed by monitoring the

morphological changes of HeLa cells incubated with RTCDs before and after  $880 \text{ nm}$  laser irradiation (Fig. 7b, c), with clear blebs (red arrow) visible after 3 min of laser irradiation compared to non-laser-irradiated cells. In addition, in the absence of the RTCDs, no changes in the cell morphology was evident after laser irradiation, suggesting that the laser used in this study was safe for non-targeted tissue and that RTCDs were required for cell death.

To further evaluate the *in vivo* effect of RTCDs for use in PTT, RTCDs were intratumorally injected into mice, followed by irradiation with an  $880 \text{ nm}$  laser for 10 min. The full-body IR thermal images show a large and rapid increase in the temperature of the tumor region, of up to  $52^\circ\text{C}$  after 6 min laser irradiation (Fig. 7d, e). This irradiation significantly inhibited tumor growth up to 16 days post-treatment (Fig. 7f).

In a recent study, nitrogen-doped RTCDs prepared from *p*-aminoazobenzene showed nucleolar targeting, intracellular ROS generation under laser irradiation, and the capacity for real-time fluorescence monitoring of dynamic changes in the nucleolus during PDT<sup>49</sup>. These characteristics encouraged the researchers to investigate the capability of the RTCDs for use in PDT. HeLa cells incubated with  $100 \mu\text{g mL}^{-1}$  RTCDs demonstrated  $>90\%$  viability in the absence of laser irradiation, compared to only 22% viability after 5 min of laser irradiation ( $638 \text{ nm}$ ,  $1 \text{ W cm}^{-2}$ ). The photoinduced cytotoxicity was attributed to the selective interaction of RTCDs with RNA in the nuclei, such that the generated ROS degrade RNA leading to cell death. Real-time fluorescence monitoring of dynamic nucleolar changes was performed throughout the process of irradiation. Reduction of nucleolar fluorescence due to degradation of RNA was accompanied by clear morphological changes consistent with apoptosis. This study provided strong validation for the potential use of RTCDs in PDT and real-time fluorescence monitoring of dynamic nucleolar changes during the therapeutic processes.

Overall, these studies demonstrated the capability of RTCDs for *in vitro* and *in vivo* phototherapeutic applications. However, challenges remain in determining the best physicochemical properties for these RTCDs to achieve optimal phototherapeutic efficacy. These properties include (i) optimal optical specifications, (ii) enhanced tumor targetability and therapeutic effect on the deep tumors, (iii) regulate the catalytic activity of RTCDs to overcome tumor hypoxia and to achieve higher treatment efficiency; all need to be addressed in future studies.

## Conclusions and outlook

In summary, RTCDs have attracted great interest from many researchers due to their biocompatibility and low toxicity, chemical inertness, excellent stability, ease of synthesis, and tunable optical properties. These properties provide a safer and less

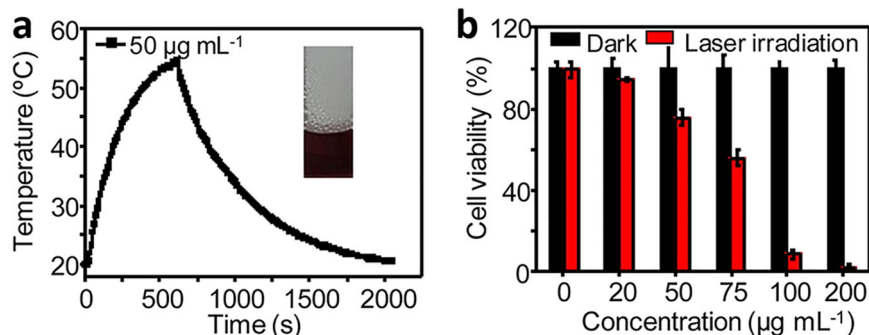


**Fig. 6** RTCDs for photodynamic therapy. **a** Photothermal effects of the RTCD water dispersion ( $50 \mu\text{g mL}^{-1}$ ) for 10 min irradiation (black line). The inset is a photograph of the RTCD aqueous dispersion after laser irradiation. **b** The viability of MCF-7 cells incubated with different concentrations of the RTCDs ( $0\text{--}200 \mu\text{g mL}^{-1}$ ) before (black bar chart) and after (red bar chart) laser irradiation for 10 min. (Fig. 6a, b adapted with permission from ref. <sup>51</sup>, Copyright 2016 American Chemical Society).



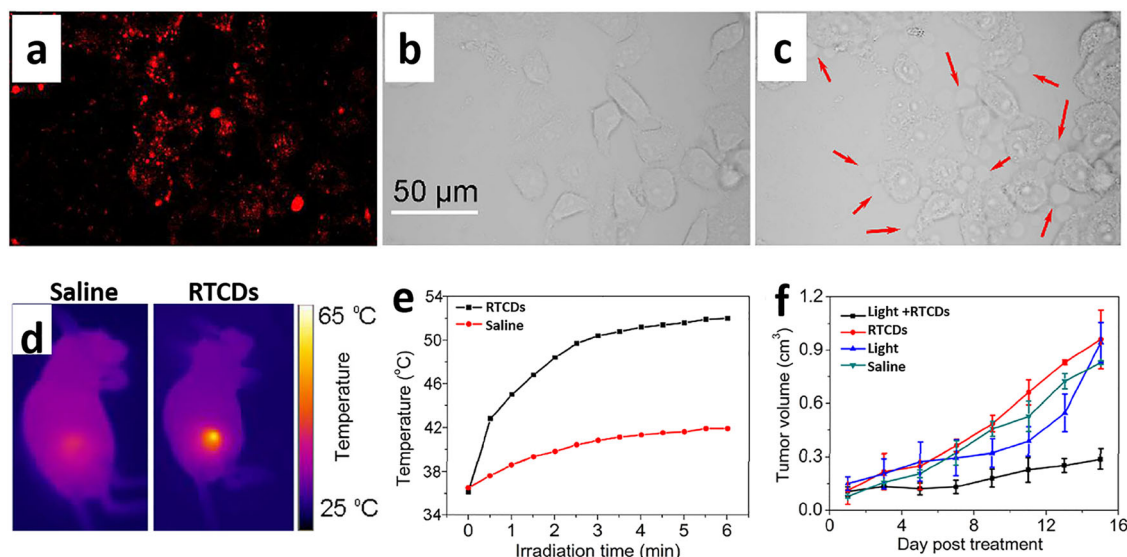


**Fig. 7 RTCDs for in vitro and in vivo photothermal therapy.** **a** Confocal fluorescent microscopic images of RTCD-treated HeLa cells under 880 nm laser excitation. Transmission electron microscopic images of HeLa cells treated with RTCDs show the morphological changes **b** before laser irradiated and **c** after 3 min of 880 nm laser irradiation (red arrows point to blebs formed around the cells after laser irradiation). All images correspond to the same region. **d** IR thermal images of 4T1 tumor-bearing mice exposed to 880 nm laser for 6 min after saline injection (80  $\mu$ L) and RTCDs (1 mg mL<sup>-1</sup>, 80  $\mu$ L). **e** Time-dependent temperature changes of tumors injected with saline (red line with dots) or RTCD aqueous solution (black line dots) after 880 nm laser irradiation. **f** Time-dependent tumor volumes after different treatments with saline (green line with downward triangles), light (blue line with upward triangles), RTCDs (red line with dots), and light and RTCDs (black line with squares). (Fig. 7a–f adapted with permission from ref. <sup>43</sup>, Copyright 2017 Springer Nature).

damaging route to enable the study and manipulation of biological systems. Here we have reviewed recent progress in the use of RTCDs as biolabels, biosensors, and phototherapeutic sensitizers.

Despite the extensive research into synthesis and characterization of CDs for a variety of applications, there is a clear gap in the literature as CDs with both red emission fluorescence and TPA capabilities (RTCDs) have not been extensively reported. Most synthesized RTCDs still have some downsides in some aspects and further modifications are required for practical requirements. The limitations are low emission intensity at longer wavelengths, poor QY and TPA cross-section, inadequate photothermal stability, and insufficient photothermal conversion efficiency. The origin and mechanisms of CD fluorescence are still under debate and thus further research to identify the cause of fluorescence is crucial to optimize the design and development of RTCDs for specific biological applications. The clear understanding of optical properties and mechanisms of RTCDs will simultaneously bring forward more information on designing CDs with TPA capabilities and provide more theoretical data for this area of study. The synthetic methods developed so far are mostly under a laboratory scale and are therefore not suitable for industrial production of RTCDs. This is due the lack of systematic studies on how various synthesis and post-synthesis parameters would affect physicochemical and biological properties of CDs, limiting their large-scale uniform production. To the best of our knowledge, there have been no reports on developing RTCD-based probes for use in fluorescence lifetime bioimaging, which can further minimize the interference of autofluorescence of biological samples and avoid the influence of experimental conditions on the fluorescence intensity and should thus be widely applicable for sensitive and accurate measurement of analytes in biosystems. Developing ratiometric RTCD-based probes as alternatives to intensity-based RTCDs probes could be a future concept for various biosensing applications. The ratiometric probes can efficiently remove the background and the fluctuation of detection conditions, thus improving the sensitivity and

accuracy of the developed probes for quantitative measurement of target elements. Further research is required in targeting RTCDs to the number of sub-cellular locations other than the cytoplasm and/or nucleus, all critical to the progress of medical research. Given the ease of post-synthetic functionalization and the well-established peptide and small-molecule targeting groups for key organelles, it should be straightforward to achieve such localization. It is also essential to design and develop RTCDs with a larger absorption coefficient to improve their in vivo phototherapeutic efficacy. Most of the reported RTCDs in literature have no absorption in second NIR region and therefore require vigorous laser light intensity for excitation to produce a competent phototherapeutic effect in the tumor site. The use of strong laser power can induce undesirable photodamage to both healthy cells and tissues.

In summary, although RTCDs have challenges in their development and use for biological applications, considering the expeditious development of the research in nanotechnology, chemistry, biology, and nanomedicine, these limitations are expected to be overcome so that RTCDs can be employed in clinical use in the near future.

Received: 1 July 2021; Accepted: 15 October 2021;  
Published online: 01 November 2021

## References

- Chen, M. & Yin, M. Design and development of fluorescent nanostructures for bioimaging. *Prog. Polym. Sci.* **39**, 365–395 (2014).
- Terai, T. & Nagano, T. Small-molecule fluorophores and fluorescent probes for bioimaging. *Pflügers Arch.* **465**, 347–359 (2013).
- Yang, Q. et al. Donor engineering for NIR-II molecular fluorophores with enhanced fluorescent performance. *J. Am. Chem. Soc.* **140**, 1715–1724 (2018).
- Chernov, K. G., Redchuk, T. A., Omelina, E. S. & Verkhusha, V. V. Near-infrared fluorescent proteins, biosensors, and optogenetic tools engineered from photochromes. *Chem. Rev.* **117**, 6423–6446 (2017).

5. Kolanowski, J. L., Liu, F. & New, E. J. Fluorescent probes for the simultaneous detection of multiple analytes in biology. *Chem. Soc. Rev.* **47**, 195–208 (2018).
6. Martynenko, I. et al. Application of semiconductor quantum dots in bioimaging and biosensing. *J. Mater. Chem. B* **5**, 6701–6727 (2017).
7. Liu, Q., Guo, B., Rao, Z., Zhang, B. & Gong, J. R. Strong two-photon-induced fluorescence from photostable, biocompatible nitrogen-doped graphene quantum dots for cellular and deep-tissue imaging. *Nano Lett.* **13**, 2436–2441 (2013).
8. Gao, X., Cui, Y., Levenson, R. M., Chung, L. W. & Nie, S. In vivo cancer targeting and imaging with semiconductor quantum dots. *Nat. Biotechnol.* **22**, 969–976 (2004).
9. Lewinski, N., Colvin, V. & Drezek, R. Cytotoxicity of nanoparticles. *Small* **4**, 26–49 (2008).
10. Liu, J. H., Yang, S. T., Chen, X. X. & Wang, H. Fluorescent carbon dots and nanodiamonds for biological imaging: preparation, application, pharmacokinetics and toxicity. *Curr. Drug Metab.* **13**, 1046–1056 (2012).
11. Wang, Y., Zhu, Y., Yu, S. & Jiang, C. Fluorescent carbon dots: rational synthesis, tunable optical properties and analytical applications. *RSC Adv.* **7**, 40973–40989 (2017).
12. Zheng, X. T., Ananthanarayanan, A., Luo, K. Q. & Chen, P. Glowing graphene quantum dots and carbon dots: properties, syntheses, and biological applications. *Small* **11**, 1620–1636 (2015). **Structural and optical characteristics of CD and their use as bioimaging and biosensing probes.**
13. Bao, X. et al. In vivo theranostics with near-infrared-emitting carbon dots—highly efficient photothermal therapy based on passive targeting after intravenous administration. *Light Sci. Appl.* **7**, 1–11 (2018).
14. Kou, X., Jiang, S., Park, S. J. & Meng, L. Y. A review: recent advances in preparations and applications of heteroatom-doped carbon quantum dots. *Dalton Trans.* **49**, 6915–6938 (2020).
15. Baker, S. N. & Baker, G. A. Luminescent carbon nanodots: emergent nanolights. *Angew. Chem. Int. Ed.* **49**, 6726–6744 (2010).
16. Lim, S. Y., Shen, W. & Gao, Z. Carbon quantum dots and their applications. *Chem. Soc. Rev.* **44**, 362–381 (2015).
17. Chu, K. W., Lee, S., Chang, C. J. & Liu, L. Recent progress of carbon dot precursors and photocatalysis applications. *Polymers* **11**, 689 (2019).
18. Hola, K. et al. Carbon dots—emerging light emitters for bioimaging, cancer therapy and optoelectronics. *Nano Today* **9**, 590–603 (2014).
19. Zuo, P., Lu, X., Sun, Z., Guo, Y. & He, H. A review on syntheses, properties, characterization and bioanalytical applications of fluorescent carbon dots. *Microchim. Acta* **183**, 519–542 (2015).
20. Webb, B. A., Chimenti, M., Jacobson, M. P. & Barber, D. L. Dysregulated pH: a perfect storm for cancer progression. *Nat. Rev. Cancer* **11**, 671–677 (2011).
21. Dong, Y., Cai, J., You, X. & Chi, Y. Sensing applications of luminescent carbon based dots. *Analyst* **140**, 7468–7486 (2015).
22. Vankayala, R. & Hwang, K. C. Near-infrared-light-activatable nanomaterial-mediated phototheranostic nanomedicines: an emerging paradigm for cancer treatment. *Adv. Mater.* **30**, 1706320 (2018).
23. Kim, S., Ohulchanskyy, T. Y., Pudavar, H. E., Pandey, R. K. & Prasad, P. N. Organically modified silica nanoparticles co-encapsulating photosensitizing drug and aggregation-enhanced two-photon absorbing fluorescent dye aggregates for two-photon photodynamic therapy. *J. Am. Chem. Soc.* **129**, 2669–2675 (2007).
24. Lesani, P. et al. Two-photon dual-emissive carbon dot-based probe: deep-tissue imaging and ultrasensitive sensing of intracellular ferric ions. *ACS Appl. Mater. Interfaces* **12**, 18395–18406 (2020).
25. Cao, L. et al. Carbon dots for multiphoton bioimaging. *J. Am. Chem. Soc.* **129**, 11318–11319 (2007).
26. So, P. T. C., Dong, C. Y., Masters, B. R. & Berland, K. M. Two-photon excitation fluorescence microscopy. *Annu. Rev. Biomed. Eng.* **2**, 399–429 (2000).
27. Juvekar, V., Park, S. J., Yoon, J. & Kim, H. M. Recent progress in the two-photon fluorescent probes for metal ions. *Coord. Chem. Rev.* **427**, 213574 (2021).
28. Kim, D., Ryu, H. G. & Ahn, K. H. Recent development of two-photon fluorescent probes for bioimaging. *Org. Biomol. Chem.* **12**, 4550–4566 (2014).
29. Zhang, X., Bloch, S., Akers, W. & Achilefu, S. Near-infrared molecular probes for in vivo imaging. *Curr. Protoc. Cytom.* **60**, 12–27 (2012).
30. Rubart, M. Two-photon microscopy of cells and tissue. *Circ. Res.* **95**, 1154–1166 (2004).
31. Benninger, R. K. & Piston, D. W. Two-photon excitation microscopy for the study of living cells and tissues. *Curr. Protoc. Cell Biol.* **Chapter 4**, Unit 4.11.1–24 (2013).
32. Oheim, M., Michael, D. J., Geisbauer, M., Madsen, D. & Chow, R. H. Principles of two-photon excitation fluorescence microscopy and other nonlinear imaging approaches. *Adv. Drug Deliv. Rev.* **58**, 788–808 (2006). **Detail study on the basic principles of nonlinear two-photon excitation fluorescence microscopy.**
33. Feng, G., Zhang, G. Q. & Ding, D. Design of superior phototheranostic agents guided by Jablonski diagrams. *Chem. Soc. Rev.* **49**, 8179–8234 (2020).
34. Kim, H. M. & Cho, B. R. Small-molecule two-photon probes for bioimaging applications. *Chem. Rev.* **115**, 5014–5055 (2015).
35. Padmanabhan, K., Andrews, S. E. & Fitzpatrick, J. A. Multi-photon imaging. *Curr. Protoc. Cytom.* **Chapter 2**, 2–9 (2010).
36. Piston, D. Imaging living cells and tissues by two-photon excitation microscopy. *Trends Cell Biol.* **9**, 66–69 (1999).
37. McVey, A. & Crain, J. Nonlinear optical methods for cellular imaging and localization. *Methods* **68**, 371–377 (2014).
38. Yamada, M., Lin, L. L. & Prow, T. W. in *Fluorescence Microscopy* (eds Cornea, A. & Conn P. M.) 185–197 (Academic Press, 2014).
39. Zipfel, W. R., Williams, R. M. & Webb, W. W. Nonlinear magic: multiphoton microscopy in the biosciences. *Nat. Biotechnol.* **21**, 1369–1377 (2003).
40. Yang, M., Li, B., Zhong, K. & Lu, Y. Photoluminescence properties of N-doped carbon dots prepared in different solvents and applications in pH sensing. *J. Mater. Sci.* **53**, 2424–2433 (2018).
41. Gharat, P. M. et al. An insight into the molecular and surface state photoluminescence of carbon dots revealed through solvent-induced modulations in their excitation wavelength dependent emission properties. *Photochem. Photobiol. Sci.* **18**, 110–119 (2019).
42. Ye, X., Xiang, Y., Wang, Q., Li, Z. & Liu, Z. A red emissive two-photon fluorescence probe based on carbon dots for intracellular pH detection. *Small* **15**, 1901673 (2019). **Development of multifunctional RTCD for two-photon imaging and sensing of pH in vitro and in vivo.**
43. Lan, M. et al. Two-photon-excited near-infrared emissive carbon dots as multifunctional agents for fluorescence imaging and photothermal therapy. *Nano Res.* **10**, 3113–3123 (2017).
44. Lu, S. et al. Near-infrared photoluminescent polymer-carbon nanodots with two-photon fluorescence. *Adv. Mater.* **29**, 1603443 (2017).
45. Wang, H. et al. Red carbon dots as label-free two-photon fluorescent nanoprobe for imaging of formaldehyde in living cells and zebrafishes. *Chin. Chem. Lett.* **31**, 759–763 (2020).
46. Bai, Y. et al. Carbon dots with absorption red-shifting for two-photon fluorescence imaging of tumor tissue pH and synergistic phototherapy. *ACS Appl. Mater. Interfaces* **13**, 35365–35375 (2021).
47. Wu, W., Zheng, T. & Tian, Y. J. C. C. An enzyme-free amplification strategy based on two-photon fluorescent carbon dots for monitoring miR-9 in live neurons and brain tissues of Alzheimer’s disease mice. *Chem. Commun.* **56**, 8083–8086 (2020).
48. Tan, C. et al. Sulfuric acid assisted preparation of red-emitting carbonized polymer dots and the application of bio-imaging. *Nanoscale Res. Lett.* **13**, 1–6 (2018).
49. Yi, S. et al. Red emissive two-photon carbon dots: photodynamic therapy in combination with real-time dynamic monitoring for the nucleolus. *Carbon* **182**, 155–166 (2021). **Efficient photodynamic therapeutic effect of RTCD with 22% HeLa cell viability after laser irradiation.**
50. Pan, L., Sun, S., Zhang, L., Jiang, K. & Lin, H. Near-infrared emissive carbon dots for two-photon fluorescence bioimaging. *Nanoscale* **8**, 17350–17356 (2016).
51. Sun, S., Zhang, L., Jiang, K., Wu, A. & Lin, H. Toward high-efficient red emissive carbon dots: facile preparation, unique properties, and applications as multifunctional theranostic agents. *Chem. Mater.* **28**, 8659–8668 (2016).
52. Li, D. et al. Thermally activated upconversion near-infrared photoluminescence from carbon dots synthesized via microwave assisted exfoliation. *Small* **15**, 1905050 (2019).
53. Liu, K. K. et al. Efficient red/near-infrared-emissive carbon nanodots with multiphoton excited upconversion fluorescence. *Adv. Sci.* **6**, 1900766 (2019).
54. Li, D. et al. Near-infrared excitation/emission and multiphoton-induced fluorescence of carbon dots. *Adv. Mater.* **30**, 1705913 (2018).
55. Jiang, L. et al. UV–Vis–NIR full-range responsive carbon dots with large multiphoton absorption cross sections and deep-red fluorescence at nucleoli and in vivo. *Small* **16**, 2000680 (2020). **Heteroatoms can significantly red-shift the emission and raise two-photon absorption efficiency of CD.**
56. Liu, J. et al. Deep red emissive carbonized polymer dots with unprecedented narrow full width at half maximum. *Adv. Mater.* **32**, 1906641 (2020).
57. Parodi, V. et al. Nonlinear optical microscopy: from fundamentals to applications in live bioimaging. *Front. Bioeng. Biotechnol.* **8**, 585363 (2020).
58. Lim, C. S. & Cho, B. R. Two-photon probes for biomedical applications. *BMB Rep.* **46**, 188–194 (2013).
59. Lesani, P. et al. Influence of carbon dot synthetic parameters on photophysical and biological properties. *Nanoscale* **13**, 11138–11149 (2021). **Influence of CD synthetic parameters on its optical properties, cellular uptake, and bioimaging ability.**
60. Fong, J. F. Y., Ng, Y. H. & Ng, S. M. in *Fullerenes, Graphene & Nanotubes* (ed. Grumezescu, A. M.) 227–295 (Elsevier, 2018).

61. Chung, Y. J., Kim, J. & Park, C. B. Photonic carbon dots as an emerging nanoagent for biomedical and healthcare applications. *ACS Nano* **14**, 6470–6497 (2020).
62. Liu, H. W., Liu, Y., Wang, P. & Zhang, X. Molecular engineering of two-photon fluorescent probes for bioimaging applications. *Methods Appl. Fluorescence* **5**, 012003 (2017).
63. Santos, C. I. et al. Selective two-photon absorption in carbon dots: a piece of the photoluminescence emission puzzle. *Nanoscale* **10**, 12505–12514 (2018). **Linear and nonlinear optical properties of CD and the nature of their emissive centre.**
64. Yao, S. & Belfield, K. D. Two-photon fluorescent probes for bioimaging. *Eur. J. Org. Chem.* **2012**, 3199–3217 (2012). **Design Considerations for developing high efficient Two-Photon excitable CDs.**
65. Wu, L., Liu, J., Li, P., Tang, B. & James, T. D. Two-photon small-molecule fluorescence-based agents for sensing, imaging, and therapy within biological systems. *Chem. Soc. Rev.* **50**, 702–734 (2021).
66. Myung Kim, H. & Rae Cho, B. Two-photon materials with large two-photon cross sections. structure-property relationship. *Chem. Commun.* **2**, 153–164 (2009).
67. He, G. S., Tan, L.-S., Zheng, Q. & Prasad, P. N. Multiphoton absorbing materials: molecular designs, characterizations, and applications. *Chem. Rev.* **108**, 1245–1330 (2008).
68. Yuan, F. et al. Shining carbon dots: synthesis and biomedical and optoelectronic applications. *Nano Today* **11**, 565–586 (2016).
69. Aratani, N., Kim, D. & Osuka, A.  $\pi$ -conjugation enlargement toward the creation of multi-porphyrinic systems with large two-photon absorption properties. *Chemistry* **4**, 1172–1182 (2009).
70. Sumalekshmy, S. et al. Design of emission ratiometric metal-ion sensors with enhanced two-photon cross section and brightness. *J. Am. Chem. Soc.* **129**, 11888–11889 (2007).
71. Tejwan, N. et al. Metal-doped and hybrid carbon dots: a comprehensive review on their synthesis and biomedical applications. *J. Controlled Release* **330**, 132–150 (2021).
72. Li, F., Yang, D. & Xu, H. Non-metal-heteroatom-doped carbon dots: synthesis and properties. *Chemistry* **25**, 1165–1176 (2019).
73. Sun, S. et al. Manganese-doped carbon dots with redshifted orange emission for enhanced fluorescence and magnetic resonance imaging. *ACS Appl. Bio Mater.* **4**, 1969–1975 (2021).
74. Manioudakis, J. et al. Effects of nitrogen-doping on the photophysical properties of carbon dots. *J. Mater. Chem. C* **7**, 853–862 (2019).
75. Zhou, J. et al. Carbon dots doped with heteroatoms for fluorescent bioimaging: a review. *Microchim. Acta* **184**, 343–368 (2017).
76. Wei, S. et al. Multi-color fluorescent carbon dots: graphitized  $sp^2$  conjugated domains and surface state energy level co-modulate band gap rather than size effects. *Chemistry* **26**, 8129–8136 (2020).
77. Gong, X. et al. Low temperature synthesis of phosphorous and nitrogen co-doped yellow fluorescent carbon dots for sensing and bioimaging. *J. Mater. Chem. B* **3**, 6813–6819 (2015).
78. Parvin, N. & Mandal, T. K. Dually emissive P, N-co-doped carbon dots for fluorescent and photoacoustic tissue imaging in living mice. *Microchim. Acta* **184**, 1117–1125 (2017).
79. Miao, P. et al. Recent advances in carbon nanodots: synthesis, properties and biomedical applications. *Nanoscale* **7**, 1586–1595 (2015).
80. Wang, J., Zhu, Y. & Wang, L. Synthesis and applications of red-emissive carbon dots. *Chem. Rec.* **19**, 2083–2094 (2019).
81. Sharma, A. & Das, J. Small molecules derived carbon dots: synthesis and applications in sensing, catalysis, imaging, and biomedicine. *J. Nanobiotechnol.* **17**, 92 (2019).
82. Zhang, J. & Yu, S. H. Carbon dots: large-scale synthesis, sensing and bioimaging. *Mater. Today* **19**, 382–393 (2016).
83. Cao, M. et al. A novel and highly stable dual-emission carbon dots-based phosphor. *J. Alloys Comp.* **873**, 159819 (2021).
84. Abbas, A. et al. Role of precursor microstructure in the development of graphene quantum dots from biomass. *J. Environ. Chem. Eng.* **9**, 106154 (2021).
85. Barman, M. K. & Patra, A. Current status and prospects on chemical structure driven photoluminescence behaviour of carbon dots. *Photochem. Photobiol. C Photochem. Rev.* **37**, 1–22 (2018). **Different Particle size distribution range can vary the HOMO-LUMO energy gaps.**
86. Noun, F., Manioudakis, J. & Naccache, R. J. P. Toward uniform optical properties of carbon dots. *Part. Part. Syst. Charact.* **37**, 2000119 (2020). **Purification profiles on a new CD system must be optimized to achieve high purity.**
87. Wu, M., Guo, H., Liu, L., Liu, Y. & Xie, L. Size-dependent cellular uptake and localization profiles of silver nanoparticles. *Int. J. Nanomed.* **14**, 4247 (2019).
88. Sukhanova, A. et al. Dependence of nanoparticle toxicity on their physical and chemical properties. *Nanoscale Res. Lett.* **13**, 1–21 (2018).
89. Yang, S. T. et al. Carbon dots as nontoxic and high-performance fluorescence imaging agents. *J. Phys. Chem. C* **113**, 18110–18114 (2009).
90. Yunus, U. et al. Targeted drug delivery systems: synthesis and in vitro bioactivity and apoptosis studies of gemcitabine-carbon dot conjugates. *Biomed. Mater.* **15**, 065004 (2020).
91. Hou, C., Wang, M., Guo, L., Jia, Q. & Ge, J. Carbon dot assemblies for enhanced cellular uptake and photothermal therapy in vitro. *ChemistrySelect* **2**, 10860–10864 (2017).
92. Havrdova, M. et al. Toxicity of carbon dots—effect of surface functionalization on the cell viability, reactive oxygen species generation and cell cycle. *Carbon* **99**, 238–248 (2016).
93. Wolfbeis, O. S. An overview of nanoparticles commonly used in fluorescent bioimaging. *Chem. Soc. Rev.* **44**, 4743–4768 (2015).
94. N. Malik, N., Arfin, T. & Khan, A. U. in *Nanomaterials for Drug Delivery and Therapy* (ed. Grumezescu, A. M.) 373–402 (Elsevier, 2019).
95. New, E. J. & Parker, D. The mechanism of cell uptake for luminescent lanthanide optical probes: the role of macropinocytosis and the effect of enhanced membrane permeability on compartmentalisation. *Org. Biomol. Chem.* **7**, 851–855 (2009).
96. Roy, R., Kumar, S., Tripathi, A., Das, M. & Dwivedi, P. Interactive threats of nanoparticles to the biological system. *Immunol. Lett.* **158**, 79–87 (2014).
97. Liu, J. H. et al. Carbon “quantum” dots for fluorescence labeling of cells. *ACS Appl. Mater. Interfaces* **7**, 19439–19445 (2015).
98. Hua, X. W., Bao, Y. W., Zeng, J. & Wu, F. Nucleolus-targeted red emissive carbon dots with polarity-sensitive and excitation-independent fluorescence emission: high-resolution cell imaging and in vivo tracking. *ACS Appl. Mater. Interfaces* **11**, 32647–32658 (2019).
99. Han, G. et al. Membrane-penetrating carbon quantum dots for imaging nucleic acid structures in live organisms. *Angew. Chem.* **58**, 7087–7091 (2019).
100. Foroozandeh, P. & Aziz, A. A. Insight into cellular uptake and intracellular trafficking of nanoparticles. *Nanoscale Res. Lett.* **13**, 1–12 (2018).
101. Thoo, L., Fahmi, M. Z., Zulkipli, I. N., Keasberry, N. & Idris, A. Interaction and cellular uptake of surface-modified carbon dot nanoparticles by J774. 1 macrophages. *Central Eur. J. Immunol.* **42**, 324 (2017).
102. Unnikrishnan, B., Wu, R.-S., Wei, S.-C., Huang, C.-C. & Chang, H.-T. Fluorescent carbon dots for selective labeling of subcellular organelles. *ACS Omega* **5**, 11248–11261 (2020).
103. Zhai, X. et al. Highly luminescent carbon nanodots by microwave-assisted pyrolysis. *Chem. Commun.* **48**, 7955–7957 (2012).
104. Lesani, P., Ardekani, S. M., Dehghani, A., Hassan, M. & Gomes, V. Excitation-independent carbon dot probes for exogenous and endogenous  $Fe^{3+}$  sensing in living cells: fluorescence lifetime and sensing mechanism. *Sensors Actuators B Chem.* **285**, 145–155 (2019). **Excitation-independent behaviour of CD and its advantages for bioimaging and biolabeling.**
105. Zhuo, Y., Miao, H., Zhong, D., Zhu, S. & Yang, X. One-step synthesis of high quantum-yield and excitation-independent emission carbon dots for cell imaging. *Mater. Lett.* **139**, 197–200 (2015).
106. Datta, K. et al. Quaternized carbon dot-modified graphene oxide for selective cell labelling—controlled nucleus and cytoplasm imaging. *Chem. Commun.* **50**, 10782–10785 (2014).
107. Qin, J. et al. Recent progress in mitochondria-targeting-based nanotechnology for cancer treatment. *Nanoscale* **13**, 7108–7118 (2021).
108. Molaie, M. J. Carbon quantum dots and their biomedical and therapeutic applications: a review. *RSC Adv.* **9**, 6460–6481 (2019).
109. Blanco, E., Shen, H. & Ferrari, M. Principles of nanoparticle design for overcoming biological barriers to drug delivery. *Nat. Biotechnol.* **33**, 941 (2015).
110. Huang, X. et al. Effect of injection routes on the biodistribution, clearance, and tumor uptake of carbon dots. *ACS Nano* **7**, 5684–5693 (2013). **CD Injection route affects the rate of blood and urine clearance, biodistribution in organs and tissues.**
111. Doria, G. et al. Noble metal nanoparticles for biosensing applications. *Sensors* **12**, 1657–1687 (2012).
112. Shibu, E. S., Hamada, M., Murase, N. & Biju, V. Nanomaterials formulations for photothermal and photodynamic therapy of cancer. *J. Photochem. Photobiol. C Photochem. Rev.* **15**, 53–72 (2013).
113. Yang, Z. et al. Advances in nanomaterials for use in photothermal and photodynamic therapeutics. *Mol. Med. Rep.* **20**, 5–15 (2019).
114. Wang, R., Li, X. & Yoon, J. Organelle-targeted photosensitizers for precision photodynamic therapy. *ACS Appl. Mater. Interfaces* **13**, 19543–19571 (2021).
115. Wu, F. et al. Porphyrin-implanted carbon nanodots for photoacoustic imaging and in vivo breast cancer ablation. *ACS Appl. Bio Mater.* **1**, 110–117 (2018).

## Acknowledgements

The authors acknowledge the Australian Research Council (Grant No. IC170100022) and the National Health and Medical Council (Grant No. APP1107470) for funding. P.L. thanks the University of Sydney for scholarship support.



### Author contributions

P.L. and H.Z. initiated this manuscript. P.L. and E.J.N. contributed to the research and discussion of all topics. P.L., supported by A.H.M.H. and E.J.N., wrote the manuscript with contributions from Z.L., S.P. and H.Z. H.Z. raised the funding that supported this study. All authors discussed and revised the manuscript and have given approval in its final version.

### Competing interests

The authors declare no competing interests.

### Additional information

**Supplementary information** The online version contains supplementary material available at <https://doi.org/10.1038/s43246-021-00214-2>.

**Correspondence** and requests for materials should be addressed to Pooria Lesani or Hala Zreiqat.

**Peer review information** *Communications Materials* thanks the anonymous reviewers for their contribution to the peer review of this work. Primary handling editors: Rona Chandrawati and John Plummer. Peer reviewer reports are available.

**Reprints and permission information** is available at <http://www.nature.com/reprints>

**Publisher's note** Springer Nature remains neutral with regard to jurisdictional claims in published maps and institutional affiliations.



**Open Access** This article is licensed under a Creative Commons Attribution 4.0 International License, which permits use, sharing, adaptation, distribution and reproduction in any medium or format, as long as you give appropriate credit to the original author(s) and the source, provide a link to the Creative Commons license, and indicate if changes were made. The images or other third party material in this article are included in the article's Creative Commons license, unless indicated otherwise in a credit line to the material. If material is not included in the article's Creative Commons license and your intended use is not permitted by statutory regulation or exceeds the permitted use, you will need to obtain permission directly from the copyright holder. To view a copy of this license, visit <http://creativecommons.org/licenses/by/4.0/>.

© The Author(s) 2021